Spatial and temporal characteristics of the fish lateral line detection

Curcic-Blake, Branislava

Chapter 5

Source location encoding in the fish lateral line canal[1]

5.1   Introduction

Fish possess the ability to detect moving and vibrating underwater objects using their mechanosensory lateral line organ (Dijkgraaf 1963). The lateral line organ is an ensemble of mechano-sensory units, called neuromasts. These units are present on the skin (superficial neuromasts) or are distributed in lateral line canals running along the body (canal neuromasts). In addition to its presence on the trunk, in many species the lateral line canal organ is also well distributed over the head in the so called cephalic lateral line canals (Coombs et al. 1988; Webb 1989). The adequate stimulus to the lateral line organ is motion of the water relative to the body, arising from nearby hydrodynamic sources. Several peripheral steps in lateral line signal transduction have been physiologically identified (reviewed in Dijkgraaf 1963; Bleckmann 1993; Coombs et al. 2000; Coombs and van Netten 2006), and biophysical models exist that accurately describe the hydrodynamical and mechanical properties of individual sensory units (reviewed in Kalmijn 1989 and van Netten 2006). To date, only a limited number of investigations have been performed to understand how the information on distance of a vibrating source is represented in the overall excitation pattern along an array of neuromasts in the lateral line canal (e.g., Denton and Gray 1982 1983; Hassan 1993; Coombs et al. 1996; Coombs and Conley 1997a,b). A precise description together with a quantitative interpretation of such measured patterns that allows a reconstruction of the location and vibration direction of vibrating sources to be made is still lacking.

The lateral line organ plays a key role in the detection of vibrating obstacles,

---

[1]Ćurčić-Blake and van Netten (2006) Source location encoding in the fish lateral line canal. J Exp Biol (accepted)

both on and under the water surface (e.g., Harris and van Bergeijk 1962; Dijkgraaf 1963; Bleckmann and Topp 1981; Kalmijn 1989; Coombs and Janssen 1990; Bleckmann 1993; Claas and Münz 1996; Coombs and Montgomery 1999). The purposes of detecting and discerning moving objects in the surrounding water are diverse and noticeably include spotting prey, predators or mates. Electrophysiological and behavioural studies have shown that an animal, using its lateral line organ, can locate an object of interest within small distances (Dijkgraaf 1963), comparable to its body length (Denton and Gray 1983; Kalmijn 1988; Coombs and Conley 1997a; 1997b; Coombs et al. 2000). In addition, behavioural studies have clearly demonstrated that animals orient their bodies according to the stimulus. The route by which fish approach a vibrating source varies between a direct heading and more indirect trajectories such as zig-zag or arched pathways and depends on the starting position of the prey (Hoekstra and Janssen 1986; Coombs and Conley 1997a).

Canals of the lateral line organ contain several neuromasts that are spatially distributed at more or less equidistant locations (e.g., Coombs et al. 1996). A single neuromast in a lateral line canal can be considered as an independent detector of the local flow pattern, because there is only minimal mechanical coupling between adjacent canal segments of fluid on either side of a neuromast (Sand 1981; Denton and Gray 1983; Tsang 1997). Moreover, single neuromasts are selectively innervated by several neurons that do not connect to other neuromasts (Münz 1985), so that local flow information, detected by a single neuromast, is relayed to higher order neurons and is therefore available for further processing by the central nervous system (CNS) (Coombs et al. 1996).

Canal neuromasts consist of mechano-sensory hair cells, covered by a gelatinous cupula that effectively transfers the motion of the fluid in the canal to the bundles of the hair cells. The directional sensitive hair cells in a neuromast are oriented with their hair bundles in opposite directions along the axis of the canal, and therefore selectively detect the component of the flow field that is parallel or anti-parallel to the canal axis (Kuiper 1956; Flock 1965). In several studies of different fish species, it has been demonstrated that the responses of the hair cells of canal neuromasts are proportional to the acceleration of the water around the fish (Denton and Gray 1983; 1989; Coombs and Janssen 1990; Kroese and Schellart 1992; Wubbels 1992; Engelmann et al. 2000). Since under free-field conditions water acceleration is proportional to the pressure gradient, the individual neuromasts encode the pressure gradients along the fish's body, as has been directly demonstrated experimentally in the trunk lateral line canal organs of goldfish (Coombs et al. 1996). It is therefore appropriate to consider the collective system of neuromasts in a lateral line canal as an array of independent pressure-gradient detectors that collects information on the surrounding flow field and has the potential to effectively image the local flow field sources around an animal (Coombs et al. 1996; Coombs and Conley 1997a,b).

Electrophysiological studies have shown that information about the location of a stimulus source is encoded in the extracellular receptor potentials (ERPs) arising from the mechano-transduction of the hair cells in a single neuromast (Harris and

van Bergeijk 1962; Sand 1989) as well as in the activity of fibres innervating the lateral line organs (Coombs et al. 1996; Coombs and Conley 1997a). So far, no direct decoding schemes have been proposed to quantitatively interpret measured excitation patterns along the lateral line canal in terms of the position and direction of vibration of sources. In order to do so, in the present study we have measured the ERPs of canal neuromasts of the ruffe (*Gymnocephalus cernuus*) in response to a vibrating sphere and we have compared the results to theoretically predicted excitation patterns along a lateral line canal. Extracellular receptor potentials are suitable for this purpose, because they can be routinely obtained and provide long and stable recordings that are necessary for mapping the associated receptive fields of a single neuromast. These quantitative results, together with the analytically modelled excitation patterns based on the properties of potential (irrotational) fluid flow past a vibrating sphere, show that the information on the sources is present in the form of a wavelet transform of the excitation pattern. This information uniquely identifies the distance and position of the sources along the lateral line, as well as their direction of vibration, within a range of roughly one fish body length. The implication of this is that the information obtained by a linear (1-D) array of detectors allows the fish to reconstruct the positions of several vibrating sources in a two-dimensional (2-D) space.

5.2 Methods and theory

5.2.1 Stimulus

In order to study the function of the lateral line in detecting the position and direction of motion of a vibrating stimulus source, extracellular receptor potentials (ERPs) were measured in response to a vibrating sphere. Figure 1 shows a diagram of the stimulus geometry in relation to the fish. The position of the sphere in the x,y-plane with respect to the fish was changed in discrete steps. The step size Δx varied between 1 and 4 mm, and the step size Δy was fixed at 5 mm; the error of both Δx and Δy was less than 50 μm. The sphere was initially placed at a short distance from the canal, at a position that was visually estimated to be closest to the cupula. All subsequent sphere positions were referenced to the coordinates of this initial position. The actual distance of the sphere from the fish in the y-direction, d, was then varied with step size Δy, and can be expressed as $d = y_\mathrm{E} + a + n\Delta y$, where y_E is an estimate of the initial distance between the edge of the sphere and the skin of the fish, a is the radius of the sphere, and n is the (positive) number of discrete steps taken in the y-direction. To obtain excitation patterns the source was displaced in the x-direction so that its position along the lateral line with respect to the neuromast, s, can be expressed as $s = b + m\Delta x$, where m is the (positive or negative) number of discrete steps taken in the x-direction (Fig. 5.1) and the initial shift of the source in the x-direction, b, was kept close to zero. The angle of the direction of vibration with respect to the lateral line (x-direction) is denoted by φ.
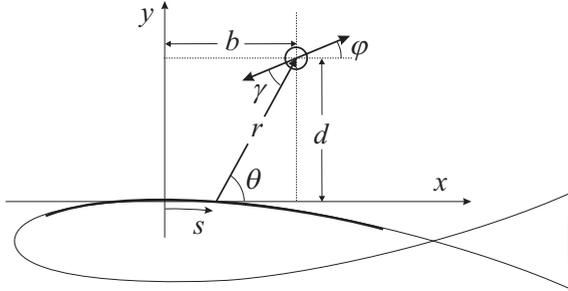
Figure 5.1: Schematic representation of the experimental setup. The horizontal x,y-plane is defined by an x-axis parallel to the lateral line, along which the position is denoted by s. A neuromast at position s is stimulated by a sphere placed at distance r and angle θ with respect to the x-axis. The distance of the sphere from the y-axis is denoted by b, and the distance from the x-axis by d. The sphere vibrates (double arrowed bold line) at an angle φ relative to the x-axis, which corresponds to an angle γ between the axis of vibration and the vector pointing to the sphere position ($\boldsymbol{r}$). For clearness the geometry is depicted in relation to the trunk lateral line system. Actual measurements were done on the cephalic lateral line system.

The hydrodynamic stimulus was produced by a Teflon sphere ($\varnothing = 2a = 10$ mm), which was attached via a stiff, insulated metal staff ($\varnothing = 4$ mm) to a piezo-electric actuator (Physik Instrumente, P-843.30) vibrating sinusoidally with a frequency of 65 or 70 Hz. These frequencies were chosen in order to evoke a cupular response in the acceleration-sensitive frequency range, well below the resonance frequency, yet enabling the measurement of a clear receptor potential. The amplitudes of vibration were kept constant during a series of steps in the x-direction, but varied from 0.5 to 3.2 μm depending on the distance to the fish. The voltage applied to the piezo-electric driver was generated via a 16-bit D-A converter (Ariel, DSP-16), so that the stimulus buffer contained 16 periods with 32 points per period. Responses were averaged corresponding to 180 stimulus buffers.

The sphere was adjusted to vibrate in a direction approximately parallel to the canal. It should be noted that due to the refraction of light at the interface of water and air, and due to the fact that the canal was covered by skin, the direction of vibration could only be roughly estimated, and thus in practice the sphere could vibrate at angles (φ) up to approximately 10° with respect to the canal axis (x-direction).

5.2.2   Preparation and measurements of extracellular receptor potentials (ERPs)

Ruffe (*Gymnocephalus cernuus*) with body lengths ranging from 10-13 cm were anaesthetised with an intraperitoneal injection of Saffan (Mallinckrodt Veterinary,

Uxbridge, UK) at a concentration of 60 mg per kg body weight. Animal procedures conformed to Dutch governmental rules and the guidelines of the University of Groningen Institutional Animal Committee (*RuG-DEC*). The fish were placed in a large water tank (base: 50 cm x 25 cm, height: 17 cm) at a depth of 2 - 2.5 cm below the water surface. They were respired by a flow of tap water through their gills and held in place by body clamps. Measurements were performed on neuromast no. 3 (Jakubowski 1963) in the supraorbital lateral line of the fish. The cupula of this neuromast is enclosed in the canal by a bony bridge, while the canal is covered by skin. A small incision was made in the skin covering the canal next to the bony bridge to allow the placement of a silver wire electrode (Ø = 0.03 mm) in the canal for measuring ERPs. The electrode was insulated except at the tip, enabling measurements of potentials from the small region around the tip, which was placed in the vicinity of the cupula. A chloridised silver reference electrode was placed in the trunk of the fish. Both electrodes were connected to a differential preamplifier (EG&G, PARC, PreAmp 113) with a band pass of 0.3 Hz – 3 kHz. The signal was further low-pass filtered (elliptic 16-pole filter (DIFA); cut-off at 16x the stimulus frequency), amplified, and stored via a 16-bit A-D converter (Ariel, DSP-16). The sampling frequency was 32 times the sinusoidal stimulus frequency. The amplitude of the ERP, the main component of which is at twice the stimulus frequency (Kuiper 1956), was obtained by calculating a Fast Fourier Transform (FFT) of the recorded ERP time traces and extracting the amplitude and phase of the component at $2f$ (130 or 140 Hz) for each discrete location of the sphere.

5.2.3   Theoretical pressure gradient patterns and wavelets

Vibrating spheres have been widely used in lateral line research (e.g., Harris and van Bergeijk 1962; van Netten and Kroese 1987; Coombs and Janssen 1990; Kroese and Schellart 1992; Coombs et al. 1996) and their usefulness in representing more general stimulus sources has been reviewed (Kalmijn 1988). For sufficiently large spheres, the flow field produced in the frequency range relevant to the lateral line system can be considered to be irrotational, so that the boundary layer around the sphere is small and the effect of viscosity can be neglected (van Netten 2006). The lateral line is assumed to be stimulated by the near-field flow of the sphere, that is, in the vicinity of the sphere, where the amplitude of the water displacement is proportional to r^{-3}, where r is the distance to the sphere (e.g., Kalmijn 1988; van Netten 2006). A sphere that vibrates with angular frequency ω and amplitude X_0, so that its displacement from equilibrium, X, is given as a function of time, t, by $X = X_0 \sin \omega t$ produces a time dependent pressure next to the lateral line canal. The (potential) pressure distribution of the near field is cylindrically symmetric around the axis of vibration and given in cylindrical coordinates by $p(r, \gamma, t) = P(r, \gamma) \sin \omega t$, with the pressure amplitude $P(r, \gamma)$ expressed as (Harris and van

Bergeijk 1962; Kalmijn 1988; van Netten 2006):

$$P(r, \gamma) = -\frac{1}{2} \rho \omega^2 a^3 X_0 \frac{\cos \gamma}{r^2}. \tag{5.1a}$$

Here ρ is the density of the fluid, a is the radius of the sphere, and γ is the angle between the direction of vibration and the line (length r) connecting a neuromast and the source (Fig. 5.1).

Canal lateral line responses are proportional to the acceleration of the external water (Denton and Gray 1983; Coombs and Janssen 1990; Kroese and Schellart 1992) which in turn, under free-field conditions, is proportional to the pressure gradient (e.g., Kalmijn 1988; van Netten 2006). The displacement of the neuromasts in a lateral line canal is therefore proportional to the local pressure gradient along the lateral line (Denton and Gray 1983; Coombs et al. 1996).

In Fig. 5.1, the lateral line canal is approximated by a straight segment along which we define the x-axis, with position variable s. The orthogonal y-axis is defined to point into the lateral direction. Further, φ denotes the angle between the direction of vibration of the sphere and the x-direction. In the Cartesian x,y-coordinate system, in which the source is located at position (b,d), we can express $P(r,\gamma)$ (Eq. 5.1a) as $P(x,y)$ by applying the following relationship:

$$\cos \gamma = \cos(\theta - \varphi) = \frac{(b-s)\cos\varphi + d\sin\varphi}{\left((b-s)^2 + d^2\right)^{\frac{1}{2}}} \tag{5.1b}$$

in which we used $\cos\theta = (b-s)/\left((b-s)^2 + d^2\right)^{\frac{1}{2}}$ and $\sin\theta = d/\left((b-s)^2 + d^2\right)^{\frac{1}{2}}$ (see Fig. 5.1). The pressure produced at position s along the lateral line in the Cartesian system, $P(s) = P(s,0)$, ($y = 0$; see Fig. 5.1) then follows from combining Eq. 5.1a with Eq. 5.1b:

$$P(s,0) = \frac{\rho \omega^2 a^3 X_0}{2} \frac{((s-b)\cos\varphi - d\sin\varphi)}{\left((s-b)^2 + d^2\right)^{\frac{3}{2}}}. \tag{5.1c}$$

The pressure gradient amplitude at lateral line position s, $\mathrm{d}P(s)/\mathrm{d}s$, (dropping the $y = 0$ in $P(s,0)$) produced by a dipole source at position b,d is then given by:

$$\frac{\mathrm{d}P(s)}{\mathrm{d}s} = C\,\Psi \tag{5.2a}$$

with:

$$\Psi = \Psi_e \cos\varphi + \Psi_o \sin\varphi\ ,$$

and

$$C = \frac{\rho \omega^2 a^3 X_0}{2d^3} \tag{5.2b}$$

and where the even and odd functions Ψ_e and Ψ_o, here termed dipole wavelets, are given by:

$$\Psi_e(\sigma) = \frac{1 - 2\sigma^2}{[1 + \sigma^2]^{\frac{5}{2}}}, \qquad \text{even dipole wavelet} \qquad (5.2c)$$

and

$$\Psi_o(\sigma) = \frac{-3\sigma}{[1 + \sigma^2]^{\frac{5}{2}}}, \qquad \text{odd dipole wavelet} \qquad (5.2d)$$

with

$$\sigma = \frac{s - b}{d} \qquad .$$

The amplitude of the pressure-gradient excitation pattern along a straight lateral line, $dP(s)/ds$, as produced by a dipole source (Eq. 5.2a), is dependent on the distance to the source, d, in two ways. Firstly, the amplitude of the pressure gradient is inversely proportional to the third power of the distance of the source to the lateral line (Eq. 5.2b). Secondly and more significantly, the spatial variations along the x-direction, as described by the even and odd dipole wavelet functions, scale linearly with the distance of the source, d, since these wavelets are exclusively dependent on the ratio of s-b to d (Eqs. 5.2c and 5.2d). Therefore, the spatial variations in pressure gradient, detected along a linear array of lateral line canal neuromasts, uniquely encode the distance, d, irrespective of the vibration amplitude, frequency, and dimensions of the source, or of the fluid properties. The parameter b determines the shift of the wavelets' points of symmetry along the lateral line. Examples of the dipole wavelet functions Ψ_e and Ψ_o are shown in Figs. 2a and 2b for two values of the source distance, d (10 and 20 mm) and with shift parameter $b = 0$. The pressure gradient consists in general of a linear combination of the even and odd wavelets, $\Psi = \Psi_e \cos\varphi + \Psi_o \sin\varphi$, depending on the direction of vibration with respect to the lateral line, φ, and with respective weight factors given by $\cos\varphi$ and $\sin\varphi$ (Eq. 5.2a). For example, Fig. 5.2c shows the linear combination of the two wavelets arising from a source at a distance of 10 and 20 mm, and $\varphi = 8°$.

The maximum amplitude of the even wavelet is reached at the point of the lateral line that is closest to the source; the odd wavelet is zero at this position. A characteristic measure of the spatial variation in excitation patterns for small angles φ (i.e., if the Eq. 5.2a becomes $\Psi \approx \Psi_e$) is the distance between the zero crossings, S (see Fig. 5.2a and 2c). It follows from Eq. 5.2c that $S = d\sqrt{2}$, so that d can be determined from measurements of S via

$$d = S/\sqrt{2} \qquad (\varphi \approx 0). \qquad (5.3a)$$

Measurements in this study were performed under the condition that the sphere vibrated parallel to the lateral line canal, such that φ is close to a zero, and Eq. 5.3a can be used (see Figs. 2a,c and 3e). Similarly, a characteristic spatial linear
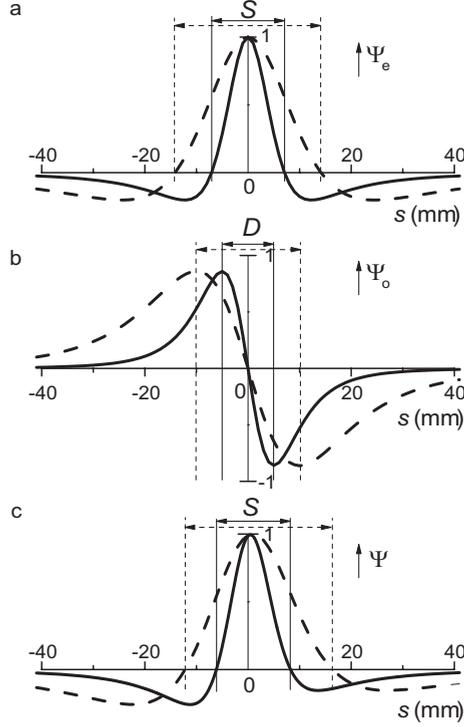
Figure 5.2: (a) The even dipole wavelet function, Ψ_e, as a function of position along the lateral line, s, for two values of the source distance d (10 mm, solid line; 20 mm, dashed line). (b) The odd dipole wavelet function, Ψ_o, for two values of the source distance d (10 mm, solid line; 20 mm, dashed line). D denotes the distance between the two extremes. (c) The linear combination of the even and odd wavelets, $\Psi = \Psi_e \cos \varphi + \Psi_o \sin \varphi$, and for $\varphi = 8°$, for two values of the source distance d (10 mm, solid line; 20 mm, dashed line). S denotes the distance along the lateral line between the zero crossings (a and c). The shift factor $b = 0$ mm in (a-c).

measure of the odd wavelet (relevant when $\varphi \approx 90°$ and the Eq. 5.2a is $\Psi \approx \Psi_o$) is the distance, D, between the maximum and minimum (see Fig. 5.2b). It is easy to show that D is equal to the distance d, so that d can be obtained from measurements via:

$$d = D(\varphi \approx 90). \tag{5.3b}$$

At intermediate angles, where both even and odd wavelets are non-zero, more complicated relations are required for estimating d (see also Discussion).

60

5.2.4 Fitting measured excitation patterns

Extracellular receptor potentials of a single neuromast were measured as a function of the position of the stimulus sphere, s, along the x-axis. An example is shown in Figs. 5.3a-c. ERPs are a measure of cupular deflection (Kuiper 1956; Harris and van Bergeijk 1962; van Netten 1987; Kroese and van Netten 1989), which in turn is proportional to the pressure gradient at the location of a neuromast and thus the ERPs can be used to monitor the local pressure gradient. In order to quantitatively describe the ERPs, we used a nonlinear transfer function based on previous combined measurements of ERPs and cupular displacements (Fig. 5.3d; from van Netten 1987). The transfer function reflects the effect of the morphological polarisation of the hair cells, which effectively results in two populations of cells with opposite directional sensitivity, being parallel or anti-parallel to the axis of the canal. As a consequence of individual hair cell rectification and saturation (e.g. Kuiper 1956; Corey and Hudspeth 1983), the collective response of the two populations is dominant at twice the stimulus frequency (Figs. 5.3b,c). The ERP amplitude, u, can then be empirically described as a nonlinear function of the cupular displacement amplitude, and thus as a function of the pressure gradient amplitude, dP/ds:

$$u(\frac{dP}{ds}) = c \left[1 - \left(1 + \left| \frac{dP}{ds} \right|^n / g \right)^{-1} \right],$$ (5.4)

where dP/ds is given by Eq. 5.2a (Fig. 5.3e). Thus, in addition to yielding the parameters d and b (e.g., Eq. 5.2a), these fits also produce values of the ERP scaling constants, g and c, and of n, which is a measure of the nonlinearity caused by saturation of the hair cells. Since the amplitude of the ERP is strongly dependent on electrode position the scaling constants (c, g and n) may vary significantly per experiment. We distinguish between experimentally controlled and fitted values of the distance by using d and d', respectively.

Figure 5.4 shows an example of a fit made with Eq. 5.4 to measurements of ERPs as a function of position s. It should be noted that the nonlinear transfer function does not affect the positions of the zero-crossings of pressure gradient excitation patterns, but merely produces local minima at these positions in the rectified response of the pressure gradient patterns as can be illustrated by comparing Fig. 5.3e with Fig. 5.2c. Fig. 5.3e was constructed from Fig. 5.2c by applying the nonlinear transfer function (Eq. 5.4) depicted in Fig. 5.3d. The phase of the pressure gradient shifts by 180° on passing a zero-crossing, as is also evident from recordings of afferent fibres (Coombs et al 1996). Since the measured ERPs are effectively rectified versions of the pressure gradients, the direction of the pressure gradient is not coded in the ERP, with the consequence that the 180° phase shifts at zero crossings are not seen in ERP recordings, as is clear from Fig. 5.4b.
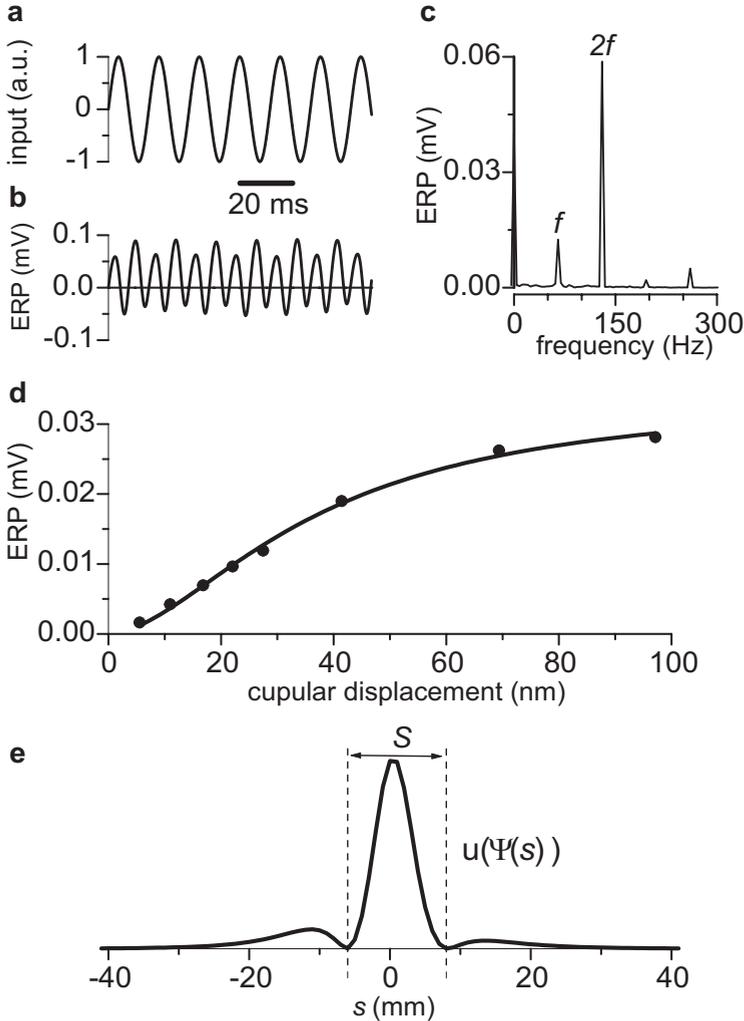
Figure 5.3: (a) Stimulus signal as a function of time, with a frequency $f = 65$ Hz. (b) ERP of a neuromast as a function of time measured in response to the signal shown in (a). (c) Spectrum of the ERP response depicted in (b) showing the amplitude components as a function of frequency. The component at twice the stimulus frequency ($2f = 130$ Hz) clearly dominates the fundamental component ($f = 65$ Hz) and is taken as the ERP amplitude. (d) Measured amplitude of the ERP ($2f$ component) as a function of cupular displacement (data points, from van Netten 1987). The non-linear model (solid line) is given by Eq. 5.4, with fitted parameters $g = 37 \pm 3$, $n = 1.7 \pm 0.2$ and $c = 34 \pm 2$. (e) ERP as a function of location along the lateral line s, simulated using the nonlinear function (Eq. 5.4) depicted in (d), applied to the pressure gradient profile calculated from the linear combination of the wavelets shown in Fig. 5.2c ($d = 10$ mm), corresponding to $\varphi = 8°$.
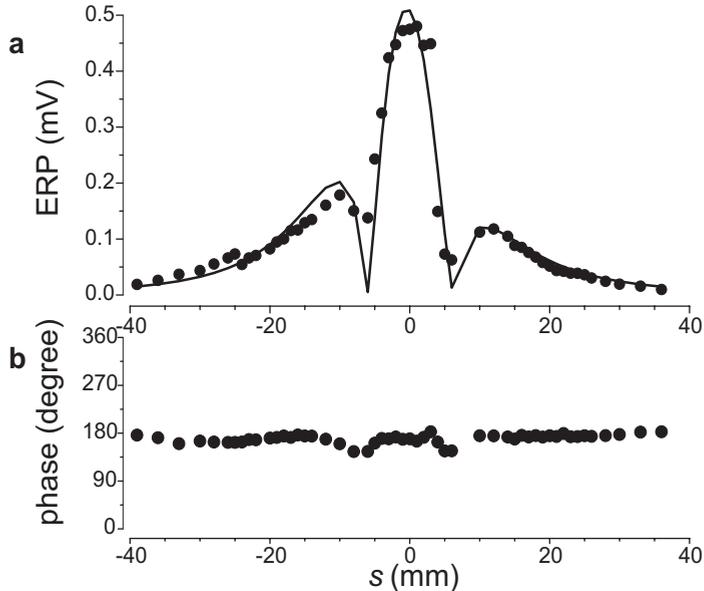
Figure 5.4: (a) Measured amplitude of ERPs (circles) from a neuromast in the supraorbital lateral line of the ruffe. The sphere was moved along an axis parallel to the lateral line (x-axis) at a distance $d = 10$ mm. This is referred to as an excitation pattern (see text). ERPs were fitted with the model given by Eq. 5.4 (solid line), describing the measured excitation patterns. ($b = $ -0.9 ± 0.2 cm; $d' = 8.5 ± 0.3$ mm; $\varphi = $ -9 ± 3°) (b) Phase of ERPs.

5.3 Results

5.3.1 Experimental quantification of linear relationship between spatial variation in pressure gradient and source distance

Extracellular receptor potentials (ERPs) of single neuromasts in the supraorbital canal of the ruffe (*Gymnocephalus cernuus*, $n = 11$) were measured to obtain quantitative information on the excitation pattern of neuromasts along the canal, as induced by a vibrating sphere. ERPs are produced by evoked transducer currents of the hair cells underlying a neuromast and are a direct measure of the mechanical displacements of a neuromast's cupula (e.g. Corey and Hudspeth 1983; Wiersinga-Post and van Netten 1998; see also *Methods*). Since cupular displacement is proportional to the external water acceleration in the approximate frequency range of 10 to 100 Hz (van Netten 2006), ERPs are thus proportional to pressure gradients at these frequencies (see Methods). Excitation patterns were obtained by varying the position of the stimulus sphere in the x-direction (cf., Fig. 5.4a). The sphere was

submerged slightly above the canal, and its position was changed in discrete steps along the x-axis at several experimentally controlled distances (d) in the y-direction (see Fig. 5.1). ERPs were plotted for each distance, d, as a function of position, s, along the lateral line canal (excitation pattern).

As the experiments were performed on neuromasts in unexposed canals, it was difficult to exactly determine the position of the cupula underneath the skin. Therefore, the centre of the peak is often slightly displaced from $s = 0$ mm as indicated by the parameter b from the fit. A typical example of an excitation pattern measured at a distance of $d = 10$ mm is shown in Fig. 5.4 (data points) together with a theoretical fit, using Eq. 5.4 combined with Eq. 5.2a (Fig. 5.4, solid line). The measured amplitudes in this example clearly peak near $s = 0$ mm, which corresponds to a sphere vibrating directly next to the cupula. The centre of the peak as determined from the fitted response appears to be at $b = $ -0.9 $\pm$ 0.2 mm.

The width of the peak, measured between the points where the amplitudes reach minimum values, is $S = 12.5$ mm. The distance d' obtained from the fitted curve is 8.5 $\pm$ 0.3 mm, while Eq. 5.3a, using $S = 12.5$ mm, yields 8.8 mm. On each side of the central peak there is a smaller one, of which the height of the left-hand peak is greater than that of the right-hand one. This difference in height can be attributed to a non-zero angle φ between the lateral line canal and the direction in which the stimulating sphere is vibrating, so that a minor contribution of the odd wavelet is required to fit the data (see Eqs. 5.2; Fig. 5.4, $\varphi = $ -9 $\pm$ 3°). Figure 5.4b presents the measured phase of the ERPs for the component at twice the stimulus frequency. It is clear that the phase is fairly constant and close to 180° along the x-axis, although small changes of up to 45° are apparent at the same positions as where the minima appear on either side of the highest peak. Similar phase changes around the minima occur in most of the measured responses.

The characteristic three-peak shape of the ERP amplitudes for small angles φ of the sphere vibration direction to the lateral line canal is maintained on varying the distance between the source and the lateral line, but the width of the peak increases with distance. Figure 5.5 demonstrates this property for two different neuromasts. Since the amplitude of the response decreases rapidly with the cube of the distance (see Eq. 5.2b), we applied at larger increased displacement amplitudes of the sphere. Therefore, the ERP excitation patterns measured at different distances are similar in amplitude, enabling the fitting of the model (Eq. 5.4) and to extract parameters with comparable accuracy. It was experimentally verified that increasing the sphere's stimulus amplitude does not affect the positions of the local minima of the ERP, which are the important features of the measured excitation patterns determining the fitted value d'.

In the examples shown in Figs. 5.5a and b, the increase of the peak width with source distance is clearly linear, as indicated by the straight dashed lines that connect the minima (i.e., pressure gradient zero-crossings) of three different excitation patterns displayed at vertically equidistant offsets. The peak width is thus proportional to the experimentally controlled distance d. This is in line with
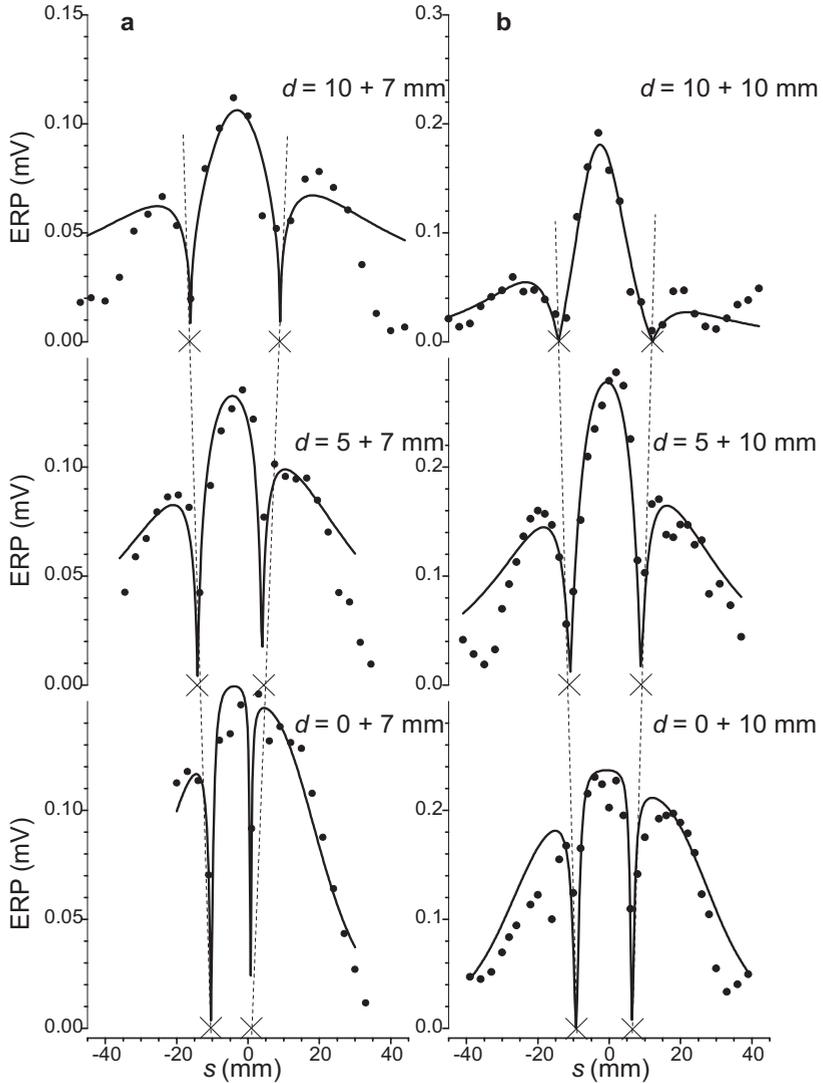
Figure 5.5: Measured excitation patterns (circles) obtained from two cupulae (a and b) with model fits (solid lines) for three different distances d of the stimulus sphere along the y axis. (a) Distances d from bottom to top are 7, 12 and 17 mm. (b) Distances d from bottom to top are 10, 15 and 20 mm. Dashed lines in both panels are fairly well intersecting the zeros of the ERPs (indicated by crosses on the equidistant x-axes) and therefore illustrate the linear widening (S; Eq. 5.3a) of the excitation patterns with increasing distance d.

theory, which predicts a linear increase of the separation, S, of the minima with increasing distance, d (Eq. 5.3a).

To further test the theoretical hypothesis of the linear relationship between the spatial variations in the excitation patterns and the experimentally controlled distance d, we compared values of d to the fitted distance parameter d'. Figure 6 5.6 shows the fitted distance d' as a function of the controlled distance d for different neuromasts ($n = 9$). A linear fit according to $d' = A_i d + B_i$ was performed on each neuromast ($i = $ 1-9). R-square values of these fits were all exceeding 0.96, supporting the hypothesized linear relationship. The coefficients A_i and B_i obtained from all neuromasts were averaged with weight factors taking the errors into account, yielding the values $A_{\mathrm{av}} = 1.07 \pm 0.01$ and $B_{\mathrm{av}} = $ -0.5 $\pm$ 0.1 mm. The associated function $d' = A_{\mathrm{av}} d + B_{\mathrm{av}}$ is plotted in the Fig. 6 5.6 (bold solid line). Fitting a linear function to the pooled data of all fish gave similar values ($A = 0.97 \pm 0.12$; $B = $ -0.7 $\pm$ 1.6 mm). For comparison a line through the origin with a slope of 1 (i.e., $d = d'$) has been added (dashed line). Together, these results firmly show the equality of experimentally controlled distance, d, and the spatial characteristics of the measured excitation patterns along the lateral line, characterised by d'.

5.3.2 Dipole imaging using the Continuous Wavelet Transform

The linear relationship between the source distance, d, and the spatial variations of pressure gradient excitation patterns, characterised by scale parameter, d', allows for an interesting and general quantitative image-reconstruction of dipole sources positions and their direction of vibration. This analysis is based on a general technique known as the Continuous Wavelet Transform (CWT). The CWT is related to the property that a function, under certain conditions, can be represented by a weighted series of scaleable base functions, or mother wavelets (e.g. Mallat 1998). The two dipole wavelets defined by Eqs. 5.2c and 5.2d, fulfil this essential feature of mother wavelets, since they are linearly scaled by the distance parameter d. In addition, mother wavelets require a second parameter, which indicates a shift of the wavelet along the x-axis. Also this parameter is defined for the dipole wavelets via b (Eqs. 5.2c,d).

The two CWTs, $F_{\mathrm{e}}(b, d)$ and $F_{\mathrm{o}}(b, d)$, of a lateral line pressure gradient excitation pattern, $f(s)$, based on the two mother wavelet functions $\Psi_{\mathrm{e}}(s, b, d)$ and $\Psi_{\mathrm{o}}(s, b, d)$ (Eqs. 5.2c,d) are then defined by:

$$F_{\mathrm{e,o}}(b, d) = \frac{1}{\sqrt{d}} \int\limits_{-\infty}^{\infty} f(s) \cdot \Psi_{\mathrm{e,o}}(s, b, d)\, ds \qquad (5.5)$$

A CWT thus consists of a convolution-like multiplication operation of the excitation pattern along the s-direction with mother wavelets, which not only have different shifts b, but also have different scales d. It can be shown (Mallat 1998) that mother
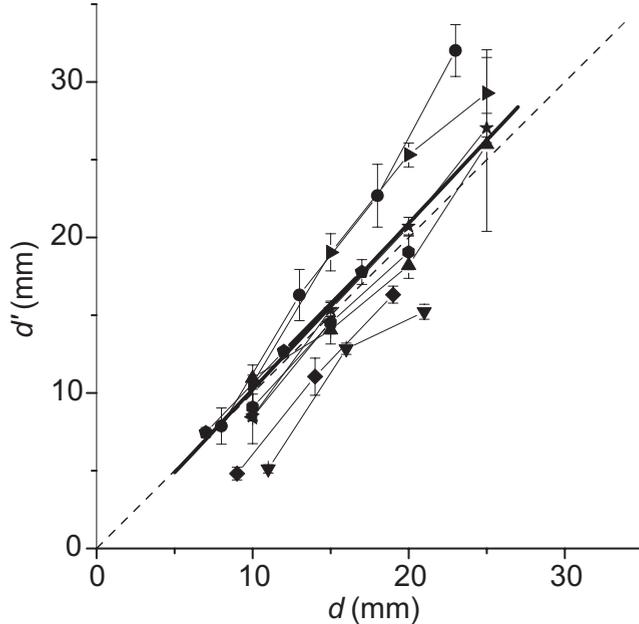
Figure 5.6: The distance d' obtained from the model (Eq. 5.4) fitted to the measured excitation patterns for $n = 9$ neuromasts (various symbols) as a function of the real distance d. The thick solid line indicates the linear fit $d' = A_{av}d + B_{av}$ with parameters $A_{av} = 1.07 \pm 0.01$ and $B_{av} = (-0.5 \pm 0.1)$ mm. For comparison, the dashed line illustrates the case $d' = d$ ($A = 1$, and $B = 0$ mm).

wavelets can be used to represent functions using the CWTs given by Eq. 5.5, under the condition of "admissibility", which requires that $\int_{-\infty}^{\infty} \Psi_{e,o}(s, b, d)\,ds = 0$. This condition is satisfied for both wavelets (Eqs. 2c,d), since they are defined as pressure gradients along a straight line, and their integral, the dipole pressure itself, vanishes at plus and minus infinity (Eq. 5.1).

The CWTs, $F_{e,o}(b, d)$, effectively form images of the dipole sources in the cylindrically symmetric 2-D b,d-plane around the lateral line along which a pressure gradient $f(s)$ is produced. This 2-D space is related to the original x,y-plane (Fig. 5.1), so that the b-direction corresponds with the x-direction and the d-direction with the y-direction. If a source is located in the x,y-plane at a certain position it shows up as a maximum of the CWT at the same location in the b,d-plane. Figure 5.7 gives examples of contour plots of CWTs that effectively image dipoles located close to (Fig. 5.7a, $d = 10$ mm) or more distant (Fig. 5.7b, $d = 30$ mm) from the lateral line. These CWTs were obtained by applying Eq. 5.5 to theoretical

pressure gradient profiles $f(s)$ (indicated below the CWT contour-plots) of dipoles vibrating in a direction parallel to the lateral line at locations indicated by white crosses in the CWT contour-plot. Figures 7a and b clearly show that the CWT analysis technique produces reliable determinations of the locations of the dipole sources by peaking at the location of the sources (white crosses). The peaks have a more elongated shape in the y-direction than in the x-direction. In addition, the shape is asymmetrical in the y-direction, so that the decline with distance from the maximum is more gradual at more remote locations. Related to this observation is that the wavelets do not form an orthogonal set of base functions; there is thus redundancy in the reconstruction in terms of individual wavelet components. This results in spatial maps in the form of peaked distributions rather than discrete peaks at the source location.

If the envelopes of excitation patterns produced by several dipole sources that are not very close to each other are combined, the CWT-reconstruction may resolve these multiple sources. An example of this is shown for two sources in Fig. 5.7c. The reconstruction is even possible if the sources are located in front of each other (Fig. 5.7d). In the latter case, the CWT image of the sources is distorted in such a way that the peaks seem to attract each other, so that the distance between the sources is underestimated.

The CWTs obtained with the even and odd mother wavelet may, in addition to the sources' positions, also provide their vibration directions, φ, via the CWT ratio which is proportional to $\tan \varphi$ (cf. Eq. 5.2a).

5.4 Discussion

We have measured and analytically modelled excitation patterns along a lateral line canal and quantitatively compared the results. Previous lateral line studies that also showed the dependence of spatial variations of lateral line excitation patterns on source distance have been limited to a more general interpretation, without quantitative decoding of the source distance and angle of vibration. We show here that the excitation patterns have characteristic shapes that can be described by a family of wavelet patterns with a linear spatial scale factor, d (see Eq. 5.2), which is equal to the distance between the source and the lateral line. This straightforward linear relationship between spatial variation in the excitation patterns and source distance allows for an unambiguous absolute coding of the source distance in a linear lateral line array. This spatial coding is very robust as it is not dependent on the characteristics of the source, such as intensity, frequency of vibration, or dimensions, nor does it rely on specific fluid properties, such as density and viscosity. These characteristics also naturally link the specific physiological features of the two direction-sensitive groups of hair cells to the operational range of the lateral line canal organ, which is typically defined as a fish's body length (Denton and Gray 1983; Kalmijn 1988; Coombs and Conley 1997a). Before elaborating on the implications of the observed linear spatial coding of source position by the lateral line
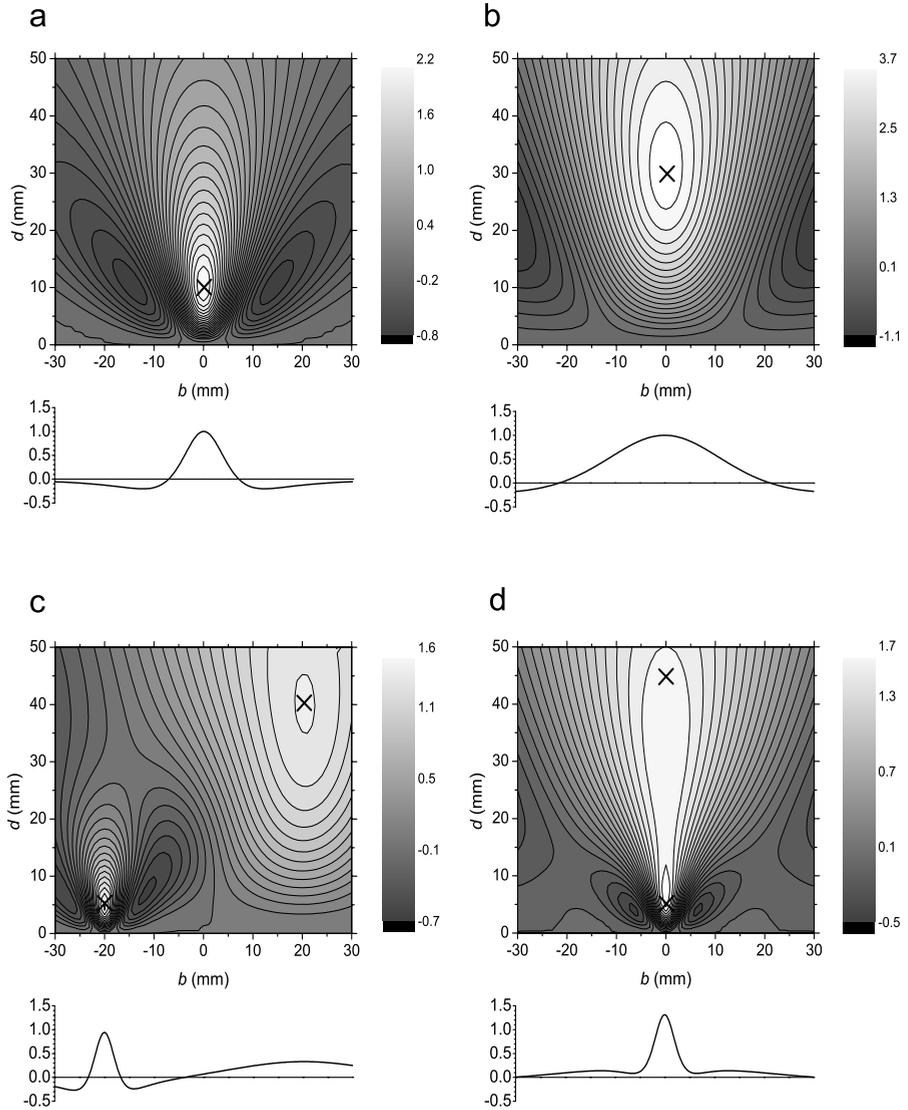
Figure 5.7: Continuous wavelet transforms (2D-contour maps) calculated using Eq. 5.5 from pressure gradient excitation profiles ($f(s)$, curves below each contour map) associated with one (a,b) or two (c,d) dipole sources. The column to the right of each contour map quantifies the contour colours. Pressure gradient profiles were obtained using a single wavelet function defined by Eq. 5.2c. For the case of two sources (c,d) the pressure gradient was determined as the sum of two individual wavelet functions. The white crosses in the contour maps indicate the positions of the dipole sources in x,y-space and correlate adequately with the maxima of the contour plots in b,d-space (panels a,b,c). If the sources are aligned with a fixed y-coordinate (panel d), the maxima seem to attract each other.

organ, we will first discuss the conditions under which the present measurements and modelling were performed and their more general relevance for excitation of the lateral line organ.

5.4.1 Relevance of dipole sources

The use of a vibrating sphere in lateral line experiments is convenient since the hydrodynamic near-field produced by the sphere can be accurately controlled and predicted. It has been shown that several types of natural stimuli can be well approximated by the sinusoidal vibration of a sphere, or dipole source. Kalmijn (1988) discussed relevant stimuli to the lateral line, describing the dipole term of the stimulus as the leading term in a series expansion of general water flow generated by moving sources that do not change their dimensions. The relevance of vibrating objects for stimulating the lateral line is supported by several experimental reports. Montgomery and Macdonald (1987) recorded the vibrations of water produced by swimming planktonic prey. They showed that these vibrations exhibited low-frequency peaks at 3-6 Hz, several harmonics of the fundamental frequency, and strong peaks between 30 and 40 Hz that were detected by the lateral line organ. Bleckmann et al. (1991) measured sinusoidal water motion presented in the vicinity of hovering fish and crustaceans. Furthermore, vibrating objects have been applied in several lateral line studies. For instance, Coombs and Janssen (1990) induced a feeding response in fish by the use of a vibrating sphere at 50 Hz. Satou et al. (1994) demonstrated that the lateral line is involved in inter-sexual communication in the himé salmon (*Onchorhynchus nerka*) by showing that a spawning response was induced by a sphere vibrating at 21 Hz. Finally, the effect of the presence of the fish in distorting a dipole field has been investigated both theoretically (Hassan 1993) and experimentally (Coombs et al. 1996), and it was shown to result in somewhat higher amplitudes but with minimal effect on the spatial characteristics of excitation patterns.

5.4.2 Suitability of ERPs of a single neuromast to analyse excitation patterns of pressure gradients along a lateral line canal

ERPs of supraorbital canal neuromasts were measured in response to sinusoidally varying displacements of water produced by a sphere. The position of the sphere was changed along a line parallel to the lateral line canal at a fixed distance (d), allowing the differences to be observed in both amplitude and phase of the ERPs arising from these different source locations. This method of using responses of a single neuromast to simulate the excitation pattern of a fixed vibrating sphere that would arise along an array of neuromasts lined up in the lateral line canal, has been used before (e.g. Coombs et al. 1996; Coombs and Conley 1997a). In the present

series of experiments ERPs were used as a monitor of cupular displacement. The displacement was not measured directly as has been done previously (van Netten and Kroese 1987; Wiersinga-Post and van Netten 2000; Ćurčić and van Netten 2005). ERPs are relatively easy to measure and require minimal invasive interference with canal- and cupular hydrodynamics, since only a small incision in the skin close to a neuromast is required for the placement of a thin wire electrode. ERPs provide hours of stable recordings, which thus allowed to obtain information of the excitation pattern with sufficient accuracy for the present quantitative analysis. The ERP increases monotonically with cupular motion (Fig. 5.3d) and is a rectified measure of cupular displacement, since the opposite groups of directionally-sensitive hair cells beneath a neuromast are fairly evenly represented (Rouse and Pickles 1991). This leads to an ERP phase ambiguity of 180°. Minima in a pressure gradient profile (Fig. 5.2c) are thus rectified to ERP maxima (cf., Fig. 5.3e), while zero crossings of the pressure gradient correlate with ERP minima. These ERP minima thus indicate a phase reversal of the pressure gradient; and their separation along the lateral line, S, is a sensitive and linear measure of the wavelet scaling parameter, d (Eq. 3e), which is not affected by the rectifying properties of the ERP. The information on distance of the source, as transduced by the two populations of hair cells and subsequently transmitted to the CNS, is thus clearly reflected in the spatial characteristics of the ERP (e.g., Fig. 5.3e). We can consequently use the ERPs to analyse the spatial encoding in an array of lateral line neuromasts.

5.4.3 Encoding of source location and direction of vibration

One of the most important questions related to source localisation by fish is how excitation patterns along the array of lateral line neuromasts can be analysed and resolved into information about the source distance. Coombs and Conley (1997b), in their behavioural experiments on mottled sculpin (*Cottus bairdi*), described several types of approach to a vibrating source that simulates prey. The approach strategy of the fish depended on its initial position with respect to the stimuli. According to these authors, the fish approached the prey along a direct route only when the prey was to the side of the fish at the onset of the stimuli. They also described a so-called arching pattern of approach that seemed to follow iso-pressure lines, and occured mainly when the fish faced the source and at 90° relative to the axis of the vibration. A zig-zag pattern of approach was observed when the fish was pointing at an angle of 45° to the source. From these observations it can be speculated that a fish might not be able to determine the location of the source in all circumstances, and that it will therefore orient its body with respect to the source in order to gain the most information.

In cases where the source vibrates in a direction parallel to the lateral line, our present analysis shows that a relatively simple strategy might work. In this situation $\varphi = 0°$, so that the pressure gradient consists only of the even wavelet function. The pressure gradient peaks at the location of the source in the x-direction. The

distance of the source in the y-direction is then simply related to the separation between the pressure gradient zero-crossings, S, according to $d = S/\sqrt{2}$ (Eq. 5.3a; Fig. 5.3e). The morphological polarisation of lateral line canal hair cells, which accounts for their directional selectivity, parallel or anti-parallel to the canal, is thus ideal for sensing the phase reversals in the excitation patterns associated with the zero-crossings (Coombs et al. 1996). If the angle of the vibration, φ, is smaller than $\sim 20°$, the distance of the source can be calculated from the distance between the zero-crossings using the above equation with an error of less than 6%.

The situation becomes more complicated when φ increases beyond $20°$. The symmetry of the three peaks in the excitation pattern changes and the main peak is no longer situated at the x-component of the source (Fig. 5.1). In fact, at increasing angles one of the side-maxima becomes smaller and practically disappears. If the vibration occurs at $90°$ to the lateral line in the x,y-plane, a symmetric pattern appears again with one pressure gradient zero crossing in between a symmetrically located maximum and minimum. The separation, D, between these two extremes is identical to the source distance (i.e., $d = D$, Eq. 5.3b).

A more robust, angle-independent and yet simple approach involves detecting the positions of the two most pronounced extremes s_{M1} and s_{M2} in the pressure gradient excitation profiles, $f(s)$ along the lateral line. If at some point in the afferent pathway the information on the locations s_{M1} and s_{M2}, can be detected and processed, a reliable distance estimate, d_{est}, can be made using $d_{est} = |s_{M1} - s_{M2}|$. The error is maximally 20% when the vibration angle is parallel to the lateral line ($\varphi = 0°$), while the estimate becomes exact for vibrations at right angles to the lateral line ($\varphi = 90°$). In the case of an arbitrary angle, the two highest maxima in the profile are close to the x-coordinate ($b \cong s_{M1} \cong s_{M2}$) of the source position, so that a simple but effective estimate of its x-coordinate is $b_{est} = (s_{M1} + s_{M2})/2$. A more reliable estimate, b_{est}, is given by a weighted sum of the positions of the maxima as follows:

$$b_{\text{est}} = \frac{f^2(s_{\text{M1}})s_{\text{M1}} + f^2(s_{\text{M2}})s_{\text{M2}}}{f^2(s_{\text{M1}}) + f^2(s_{\text{M2}})}$$

It can be shown that the error in this estimate of the x-coordinate is always less than 5% of the (real) source distance, d, independent of φ.

The CWT analysis presented here is a more general technique that can be applied if the axes of vibration are not known and if multiple sources contribute to an excitation pattern. It is somewhat more elaborate than the estimates just discussed, but it effectively produces a complete 2-D image of the sources present in the space around a lateral line. The ratio of the reconstructions based on the even and odd mother wavelets may give the angle of vibration, φ. However, it is not known whether neural stages of lateral line signal processing exist in which correlates of the scaled convolution-like algorithm (Eq. 5.5) are performed. Convolution-like processing or the cross-correlating of signals has been incorporated in models of

direction detection by the superficial lateral line system (Franosch et al. 2003) and, in combination with neural delay lines, in models of directional hearing (Knudsen et al. 1987).

A general statement that can be made on the basis of the CWT reconstruction is that a fish, by observing a one-dimensional pressure gradient pattern along its lateral line, in principle has the information necessary to determine the position of sources and their axes of vibration in a 2-D plane through the lateral line canal. This extension from one to two dimensions is made fundamentally possible by the restrictions of the hydrodynamic field having properties of (potential) flow. This gives rise to the linear relationship between the source distance and the spatial scaling factor d. A combination of differently oriented lateral lines, which are found in particular on the head (Coombs et al. 1988; Webb 1989), will therefore allow for another dimensional extension, resulting in an effective local 3-D reconstruction of source locations.

5.4.4 Accuracy and operational range of source position detection

It is possible to derive an interesting upper limit on the operational range within which the parameter d, and therefore the distance of a source, can be decoded, when the coding relies on the detection of phase reversal in the excitation patterns. It has been suggested (Coombs et al. 1996) that the lateral line system, with its two morphological populations of directionally sensitive hair cells, is ideally equipped for such a task. The largest distance between two phase reversals in an array of lateral line detectors is limited to its overall length L and imposes a maximum on the operational detection range of $L/\sqrt{2}$ for parallel vibrations (Eq. 5.3a). Our measurements were done on the cephalic lateral line where the lengths of the canal are shorter than those along the trunk. We can however expect the detection range of the trunk canal to be the maximum that a fish may obtain using the lateral line system, making the overall maximum detection range comparable to a fish' body length. It has indeed been reported that the operational range of distance detection is of the order of a body length (Denton and Gray 1983; Kalmijn 1988; Coombs and Conley 1997a; see also Coombs and Montgomery 1999), in line with the above notion, although experimental data on operational range across fish with different lengths are scarce. The operational range cannot solely depend on the fish length since the fluid acceleration to be detected by the neuromasts needs to reach a threshold value of the order of 1 mm/s^2 (ruffe), which is equivalent to pressure gradients of the order of mPa/mm (e.g. van Netten 2006). In addition to the vibration amplitude and frequency, the dimensions of the source in relation to its distance from the lateral line thus determine whether a sufficient signal-to-noise ratio is achieved in an array of neuromasts along a lateral line canal in order to allow a reliable reconstruction of the source's position (Eq. 5.2b).

So far, only continuous pressure gradient profiles have been considered. In the

lateral line canal pressure gradient profiles are sampled at the discrete positions where neuromasts are present. The related sampling distance, or inter-neuromast distance, D_n, thus imposes limits on the accuracy with which the position of a source can be detected. The spatial frequencies of the dipole wavelets scale inversely with the distance of the source to the lateral line, d. Taking $2/d$ as the spatial frequency bandwidth of a wavelet produced by a source at a distance d, a range in which most of its energy appears to be contained, Nyquist's criterium requires a sampling distance of $d/2$ or less to reliably detect the spatial characteristics of this wavelet. This means that a source, to be correctly detected, should not be closer than approximately twice the inter-neuromast distance D_n. Relative short stretches of lateral line canals in different orientations found on the head are therefore expected to enable mapping of a 3-D space limited to the region close to the head and mouth, and with a resolution determined by the neuromast density.

The present analysis has been based on the detection of pressure gradients along linear arrays. Lateral line arrays usually have some curvature, depending on their location. For the trunk lateral line this is most likely causing only small deviations, but shorter lateral line canal arrays, such as those on the animal's head usually have more curvature, which will likely affect the accuracy of the results of a CWT-analysis, as presented. Nevertheless, the strongest variations in pressure gradients will occur at the neuromasts along the lateral line closest to the source, which in a CWT-like analysis provide the dominant information on the source position along the array.

In conclusion, dipole sources vibrating with sufficient amplitude can be detected if their distance, d lies within a range having a lower limit determined by twice the inter-neuromast distance and an upper limit of the order of the length of the lateral line canal array, L ($2D_n < d < \frac{L}{\sqrt{2}}$).